The Astronomical Journal, 145:21 (11pp), 2013 January doi:10.1088/0004-6256/145/1/21

THE MASS OF THE BLACK HOLE IN XTE J1118+480

Juthika Khargharia[1], Cynthia S. Froning[2,5], Edward L. Robinson[3], and Dawn M. Gelino[4]
[1] SAS Institute Inc., 820 SAS Campus Dr., Cary, NC 27513, USA; juthikak@gmail.com
[2] Astrophysical and Planetary Sciences, University of Colorado, 391 UCB, Boulder, CO 80309, USA; cynthia.froning@colorado.edu
[3] Department of Astronomy, University of Texas at Austin, Austin, TX 78712, USA; elr@astro.as.utexas.edu
[4] NASA Exoplanet Science Institute, Caltech, 770 South Wilson Avenue, Pasadena, CA 91125, USA; dawn@ipac.caltech.edu
Received 2012 September 21; accepted 2012 November 7; published 2012 December 12

ABSTRACT

We present contemporaneous, broadband, near-infrared spectroscopy (0.9–2.45 μm) and *H*-band photometry of the black hole X-ray binary, XTE J1118+480. We determined the fractional dilution of the NIR ellipsoidal light curves of the donor star from other emission sources in the system by comparing the absorption features in the spectrum with field stars of known spectral type. We constrained the donor star spectral type to K7 V–M1 V and determined that the donor star contributed 54% ± 27% of the *H*-band flux at the epoch of our observations. This result underscores the conclusion that the donor star cannot be assumed to be the only NIR emission source in quiescent X-ray binaries. The *H*-band light curve shows a double-humped asymmetric modulation with extra flux at orbital phase 0.75. The light curve was fitted with a donor star model light curve, taking into account a constant second flux component based on the dilution analysis. We also fitted models that included emission from the donor star, a constant component from the accretion disk, and a phase-variable component from the bright spot where the mass accretion stream impacts the disk. These simple models with reasonable estimates for the component physical parameters can fully account for the observed light curve, including the extra emission at phase 0.75. From our fits, we constrained the binary inclination to $68^\circ \leqslant i \leqslant 79^\circ$. This leads to a black hole mass of $6.9\ M_\odot \leqslant\ M_{\rm BH} \leqslant 8.2\ M_\odot$. Long-term variations in the NIR light curve shape in XTE J1118+480 are similar to those seen in other X-ray binaries and demonstrate the presence of continued activity and variability in these systems even when in full quiescence.

Key words: binaries: close – black hole physics – infrared: stars – stars: individual (XTE J1118+480)

Online-only material: color figures

1. INTRODUCTION

XTE J1118+480 belongs to the class of transient low mass X-ray binaries (LMXBs) in which a late-type donor star transfers mass to its compact companion (either a black hole or a neutron star) through an accretion disk. It was discovered by the All-Sky Monitor aboard the *Rossi X-ray Timing Explorer* satellite when it went into outburst in 2000 (Remillard et al. 2000). Because of its location along a sightline of low interstellar absorption ($E[B-V] = 0.013$), this system has been extensively studied both in outburst and in quiescence at multiple wavelengths (e.g., Hynes et al. 2000; McClintock et al. 2001b; Fender et al. 2001; Chaty et al. 2003). Observations obtained during outburst and after the system had returned to quiescence established several dynamical properties of the binary, including its orbital period ($P_{\rm orb} = 0.17$ days), donor star radial velocity semi-amplitude ($K_2 = 709$ km s^{-1}), and a mass function of the compact accretor of $f(M) = 6.27 \pm .04\ M_\odot$ (McClintock et al. 2001a; Wagner et al. 2001; Gonzalez Hernandez et al. 2008). The mass function is the minimum mass of the compact object, establishing that XTE J1118+480 contains a black hole.

Accurate compact object masses are required to test models of formation and evolution of black holes and neutron stars (Brown et al. 1998; Fryer & Kalogera 2001; Nelemans & van dan Heuval 2001; Belczynski et al. 2012). A black hole is characterized by its mass and spin, and a reliable estimate of the latter is intricately dependent on the former (e.g., Steiner et al. 2009). These two parameters are critical in understanding space–time behavior near a black hole (McClintock et al. 2011). X-ray binaries with black hole accretors have been used to test accretion disk and jet models (Yuan et al. 2005; Maitra et al. 2009), to test models of natal kicks and spin–orbit misalignments between the black hole and the accretion disk (Fragos et al. 2009), and to predict observational tests of braneworld gravity models (Johannsen 2009). Observations of black holes in X-ray binaries are also important for understanding supermassive black holes in active galactic nuclei (AGNs). Studies have revealed a "Fundamental Plane" of black hole accretion in which X-ray luminosity, radio luminosity, and black mass are related, both for Galactic black holes and their supermassive counterparts, implying that physical processes in AGNs can be illuminated by observations of similar processes in X-ray binaries by an appropriate scaling of the black hole mass (Merloni et al. 2003; Falcke et al. 2004).

Compact object mass determinations require values for the binary orbital period, the radial velocity semi-amplitude of the donor star, the mass ratio, and the inclination. The latter is usually determined by modeling the ellipsoidal modulation of the light curve caused by the Roche lobe-filling donor star. The light curve observations are often performed in the near-infrared (NIR), where the late-type donor star dominates. Many investigators have assumed a negligible contribution from non-stellar sources (e.g., the accretion disk and/or a jet outflow) at NIR wavelengths. However, this assumption has been questioned based on fits to the NIR spectra with donor star templates and on variability in the NIR light curves during quiescence (Froning et al. 2007; Reynolds et al. 2008; Cantrell et al. 2008, 2010). Unaccounted-for extra flux will lower the derived binary inclination from its true value and consequently overestimate the compact object mass, so accurate determinations of the relative contributions of the donor star and

[5] Center for Astrophysics and Space Astronomy, University of Colorado, 593 UCB, Boulder, CO 80309-0593, USA.

other emitters in the NIR are necessary to obtain correct mass values. In a recent study of the effects of systematic errors on the derived masses of black holes in X-ray transients, Kreidberg et al. (2012) showed that the assumption of zero non-stellar light biases derived black hole masses to higher than their true values, often by significant amounts. They also cautioned that the non-stellar component often varies over time and with orbital phase, requiring careful modeling of the observed light curve and contemporaneous acquisition of light curve and spectroscopic data to obtain unbiased compact object masses.

Gelino et al. (2006) obtained the most comprehensive light curve data set for XTE J1118+480, covering the *B, V, R, J, H,* and *K* wavebands. They simultaneously modeled all the light curves to derive an inclination of $68^{+2.8}_{-2.0}$ deg and a black hole mass of $M_{\rm BH} = 8.53 \pm 0.6\ M_{\odot}$. However, they assumed that the non-stellar contribution in the NIR was negligible, <8% dilution of the donor star light. Their inclination value was lower than the values found by other investigators (ranging from 71° to 82°) using a variety of analysis methods, which may be due to Gelino et al.'s assumption of negligible non-stellar flux in the NIR (Wagner et al. 2001; Zurita et al. 2002; Mikolajewska et al. 2005; Khruzina et al. 2005). Changes in the shape of the NIR light curve over short time periods—the *J*-band light curve taken by Mikolajewska et al. (2005) shows uneven peaks, unlike the symmetric ones seen by Gelino et al. (2006) five months earlier—suggest that variable, non-stellar emission is in fact present in XTE J1118+480 in the NIR.

Motivated by the goal of determining an accurate black hole mass in XTE J1118+480, we obtained contemporaneous light curve and spectral data of this system at NIR wavelengths to establish the non-stellar dilution from spectroscopy at the time of acquisition of the light curve so that the true binary inclination of the system can be obtained. In the following sections, we estimate the veiling caused by the non-stellar components at NIR wavelengths by examining the broadband spectral energy distribution (SED) and by measuring the equivalent widths of absorption lines in the photosphere of the donor star compared to field stars of known spectral type. We account for the extra NIR light when fitting ellipsoidal models to the observed light curve data in order to obtain a robust value of binary inclination and consequently determine the black hole mass.

2. OBSERVATIONS

We obtained contemporaneous spectroscopic and photometric observations of XTE J1118+480 using the Gemini Near-Infrared Spectrograph (GNIRS) at Gemini-North and the Near-Infrared Camera & Fabry–Perot Spectrometer (NICFPS) on the 3.5 m telescope at Apache Point Observatory (APO). Photometry and spectroscopy were initially scheduled to be acquired on 2011 April 2 and 3 at both locations. We observed successfully at both sites on April 2. Additional light curve data were obtained on April 3 but due to bad weather at Mauna Kea, we did not complete the spectral observations until April 12. Table 1 lists the observations, exposure times, and orbital phase coverage for the program.

2.1. Spectroscopy

We observed XTE J1118+480 using GNIRS at Gemini-North (Elias et al. 2006). GNIRS was configured in the cross-dispersed mode with the 31.7 line mm^{-1} grating and the 0.″30 wide slit, yielding $R \sim 1700$ while effectively covering the near-infrared range from 0.9 to 2.5 μm. We obtained a total on-source observing time of 4.2 hr. Data were taken in ABBA pairs at two positions along the 7.″0 long slit with a 310 s exposure time at each position. The slit was oriented along the mean parallactic angle throughout the observations. An A0 V type telluric star was observed hourly with the same configuration. From two nights of data, we were able to cover all binary phases at least once, except phases $\phi = 0.10$–0.35 and $\phi = 0.72$–0.76, which were covered twice. The raw data were reduced using the GNIRS tools within the Gemini-IRAF package, version v1.11. The raw images were first treated for fixed pattern noise using the `cleanir`[6] tool. The other data reduction steps consisted of flat fielding, sky subtraction, and wavelength calibration. Owing to the faintness of the target, we could not confidently extract the spectra from the individual sky-subtracted exposures. Instead, we combined every three exposures (adjacent in phase and equivalent to 5% of one full orbit) to perform reliable spectral extraction. The spectra extracted in this manner were minimally affected by orbital smearing effects when compared with the instrumental resolution of 177 km s^{-1}. Flux calibration and telluric correction were performed with the `xtellcor` package within Spextool (version 3.4; Cushing et al. 2004; Vacca et al. 2003). We shifted each of the extracted spectra to the rest frame of the donor star using the orbital ephemeris of Calvelo et al. (2009), median-combined each order separately, and merged all of the orders to generate the time-averaged spectrum of XTE J1118+480, which is shown in Figure 1. The spectrum has been boxcar-smoothed by 2 pixels, corresponding to one resolution element. The spectrum in Figure 1 was corrected for interstellar absorption using $A_V = 0.066$ (Gelino et al. 2006). We did not attempt to quantify the flux-calibration accuracy since the spectral analysis of XTE J1118+480 does not require absolute flux values. However, we find that the mean *H*-band flux of the spectrum agrees with the photometry within ∼4%.

Table 1
Observations of XTE J1118+480

	Date	Individual $t_{\rm exp}$ (s)	Total $t_{\rm obs}$ (hr)	Orbital Phase Coverage
Spectroscopy	04/02/11	310	2.1	0.13–0.39, 0.72–0.98
	04/12/11	310	2.1	0.06–0.32, 0.49–0.76
Photometry	04/02/11	20	4.0	0.00–0.35, 0.40–0.99
	04/03/11	20	3.4[a]	0.18–0.99, 0.01–0.04

Note. [a] Data after the two hours of observation were discarded owing to bad weather.

2.2. Photometry

We obtained *H*-band light curve data with NICFPS at APO (Hearty et al. 2005). We used individual exposure times of 20 s for the target. A standard star for flux calibration was observed every 1.5 hr. We had excellent seeing conditions (∼0.″6) on the night of April 2, but on April 3 the seeing conditions went from moderate (∼0.″8) to poor (>1.″0) after the first two hours of observing and the data were discarded. The binary orbital phases between $\phi = 0.1$–0.2 and $\phi = 0.33$–0.5 were not covered at all, but all other phases were covered more than once. To account for the dark current in the NICFPS exposures, dark frames matching the exposure times of the target and standard star were obtained at the beginning of each observing run and subtracted from the target/standard star exposures. Finally, the images were flat-fielded with sky-flats. We obtained five point dither images of

[6] http://staff.gemini.edu/~astephens/niri/cleanir/

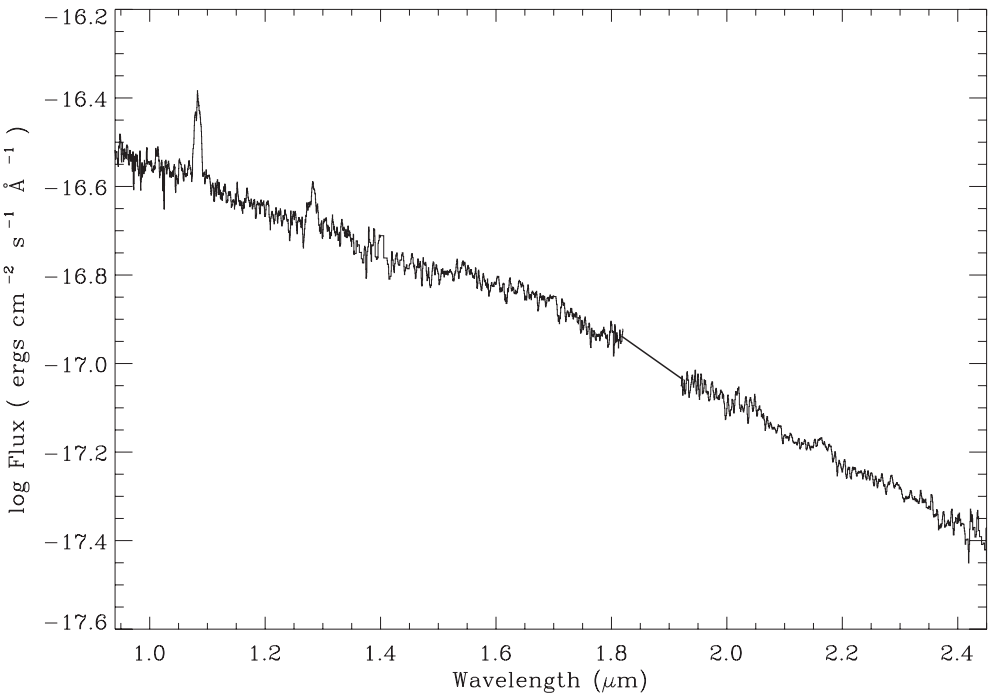

Figure 1. Time-averaged spectrum of XTE J1118+480 obtained after correcting for atmospheric absorption and shifting the individual exposures to the rest frame of the donor star. The dereddened spectrum is shown. the SpeX short cross-dispersed observing mode does not cover the wavelength region from 1.86 to 1.93 μm, which is indicated by a straightline in the figure.

the field, each offset by 20″, and constructed a sky-flat by median combining these exposures. To obtain sufficient signal-to-noise ratio (S/N) in our reduced data images, we median combined every three exposures (equivalent to ∼60 s) to construct final reduced images. Aperture photometry was performed on the combined images using the IRAF `phot` package. For flux calibration, we used the stars in the field of XTE J1118+480 selected from the Two Micron Sky Survey catalog as well as the ARNICA (Arcetri NICMOS3 camera) near-infrared standard star AS-11 (Hunt et al. 1998).

3. ANALYSIS

3.1. The Donor Star Spectral Type and Fractional Contribution to the NIR Spectrum

The spectrum of XTE J1118+480 displays narrow absorption lines of neutral metals, including transitions of Al I, Na I, Mg I, Fe I, and Si I that are believed to originate in the photosphere of the donor star. We also detect broad emission lines of H I and He I from the accretion disk. The *J*-, *H*-, and *K*-band spectra are shown in Figures 2–4. The error bars shown were calculated for each resolution element (2 pixels) by fitting straight lines through several continuum-dominated regions and obtaining the rms scatter about the fit. The continuum-dominated regions were selected after an inspection of similar regions in K5 V–M1 V template stars. We obtained S/N estimates of ∼18 in the *H* band and ∼15 in the *J* and *K* bands, respectively.

In the *J* band, we detect a few absorption features in the 1.175–1.320 μm range, mainly blends of Mg I, Si I, Fe I, and Al I, and broad emission features of H I and He I. In the *H* band, we observe narrow atomic features of Mg I, Al I, and Si I. In the *K* band, the most prominent features used for spectral classification are the ^{12}CO bands, Na I, and Ca I, with Na I. The position of these lines is marked in Figure 4. There is also a weak emission feature of H I at 2.16 μm. Most of the absorption features are detected at low confidence or undetected in K. We do not detect any CO features in the *K* band. Enhanced N V and depleted C IV and O V emission lines have been seen in the UV spectrum of XTE J1118+480, suggesting that the accreting material has been CNO processed (Haswell et al. 2002). Therefore, our non-detection of the CO-bands in the *K* band is unsurprising. In the *H* band, we apparently detect the ^{12}CO (6,3) feature at 1.619 μm, but given the relative oscillator strengths of the *K*- and *H*-band lines (the second overtone, $\Delta v = 3$, bands of CO near the 1.1619 μm have oscillator strengths that are approximately 100 times smaller than the first overtone bands near 2.29 μm) and the presence of several other species contributing features in this wavelength region (including Ca, Fe, Ni, Si, and OH), we consider the apparent *H*-band CO feature to be spurious.

The spectral type of the donor star in XTE J1118+480 has been broadly classified as K5 V–M1 V (Gonzalez Hernandez et al. 2008; Gelino et al. 2006; Wagner et al. 2001; Frontera et al. 2001; McClintock et al. 2001b). To obtain a precise black hole mass, we want to constrain the spectral type of the donor star further and to estimate the relative contributions of NIR light from the donor star and other sources in the system. Toward that end, we examined the broadband SED of XTE J1118+480 compared to field stars. Figure 5 shows the spectrum of XTE J1118+480 compared to the spectrum of a K5 V star (in red) and an M1 V star (in green). The broad *H*-band bump (between 1.5 and 1.7 μm) that is seen in the spectra of K-stars increases in amplitude with decreasing effective temperature and is attributed to the H^- opacity minimum at 1.6 μm (Rayner et al. 2009). In XTE J1118+480, the size of this feature is consistent with a donor star spectral type later than K5 V.

Earlier studies assumed that the donor star is the sole source of NIR emission in XTE J1118+480. If we follow that assumption and scale the field star spectra to match the observed flux in *K* (at 2.23 μm), then we find that the template field star

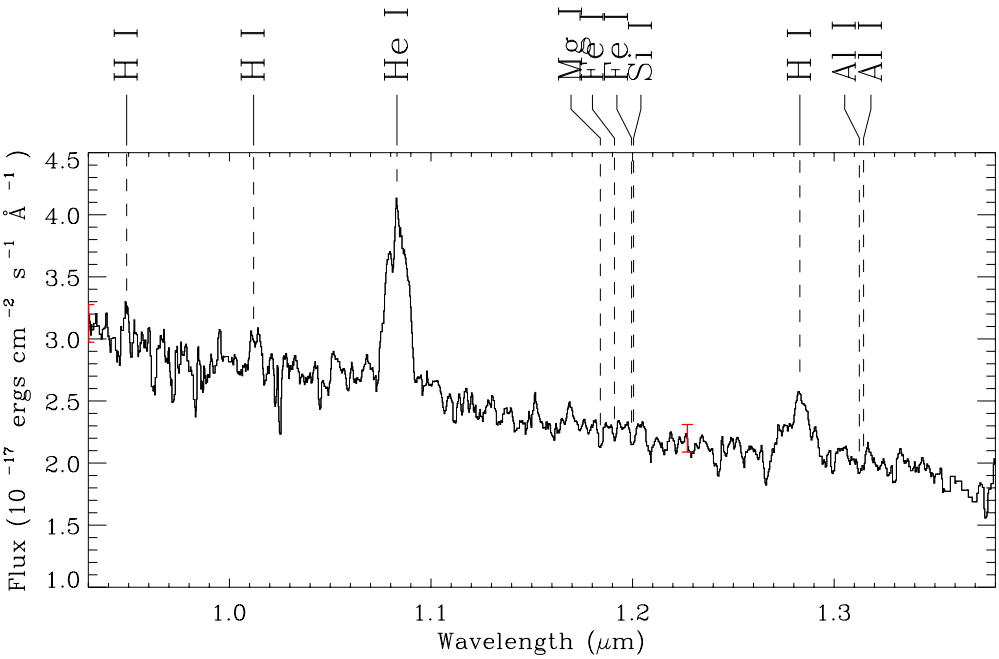

Figure 2. *J*-band spectrum of XTE J1118+480 showing emission features from the accretion disk and absorption features from the donor star. The typical error bar is shown in red.

(A color version of this figure is available in the online journal.)

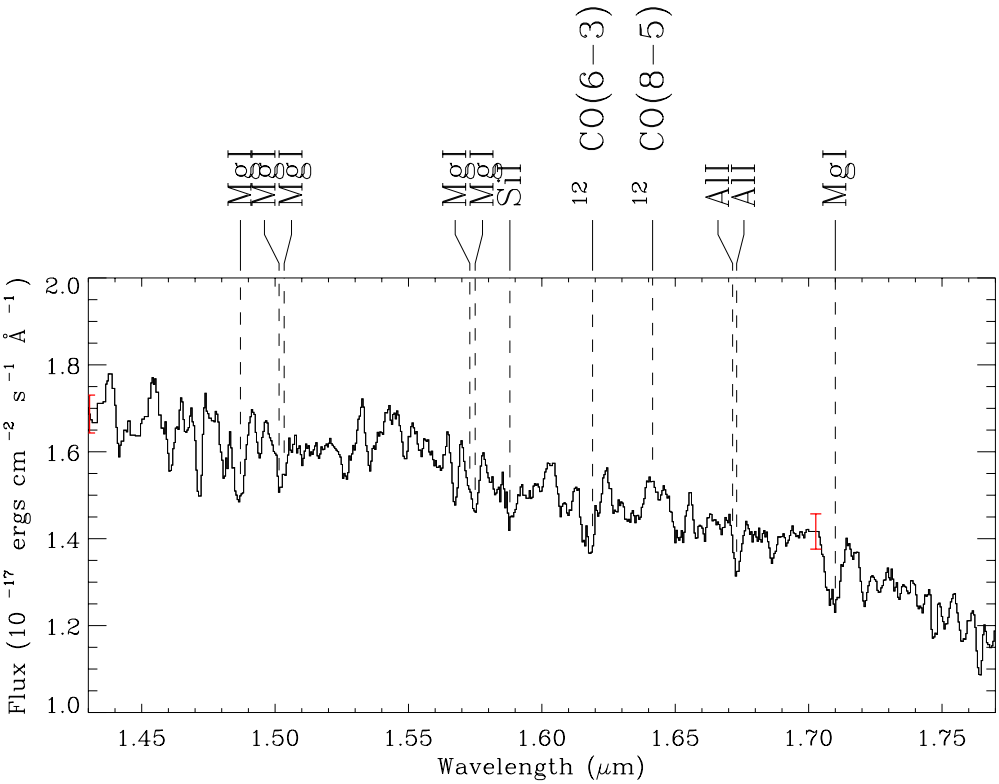

Figure 3. *H*-band spectrum of XTE J1118+480.

(A color version of this figure is available in the online journal.)

spectrum unphysically exceeds the observed spectrum at shorter wavelengths (>7% in both *J* and *H*) for K7 V or earlier spectral types. Thus, some dilution of the donor star flux is required if the spectral type is K7 V or earlier. Based solely on the broad spectral shape, an MI V or later donor spectral type could be responsible for most or all of the NIR flux, at least for wavelengths >1.5 μm.

To constrain the donor spectral type further and estimate the fraction of NIR flux originating from the donor star (donor fraction, *f*) in XTE J1118+480, we followed the procedure outlined in Khargharia et al. (2010) and Froning et al. (2007). Specifically, we fit normalized template spectra of known spectral type to the normalized spectrum of XTE J1118+480. Dilution of the X-ray binary spectrum by non-stellar emission

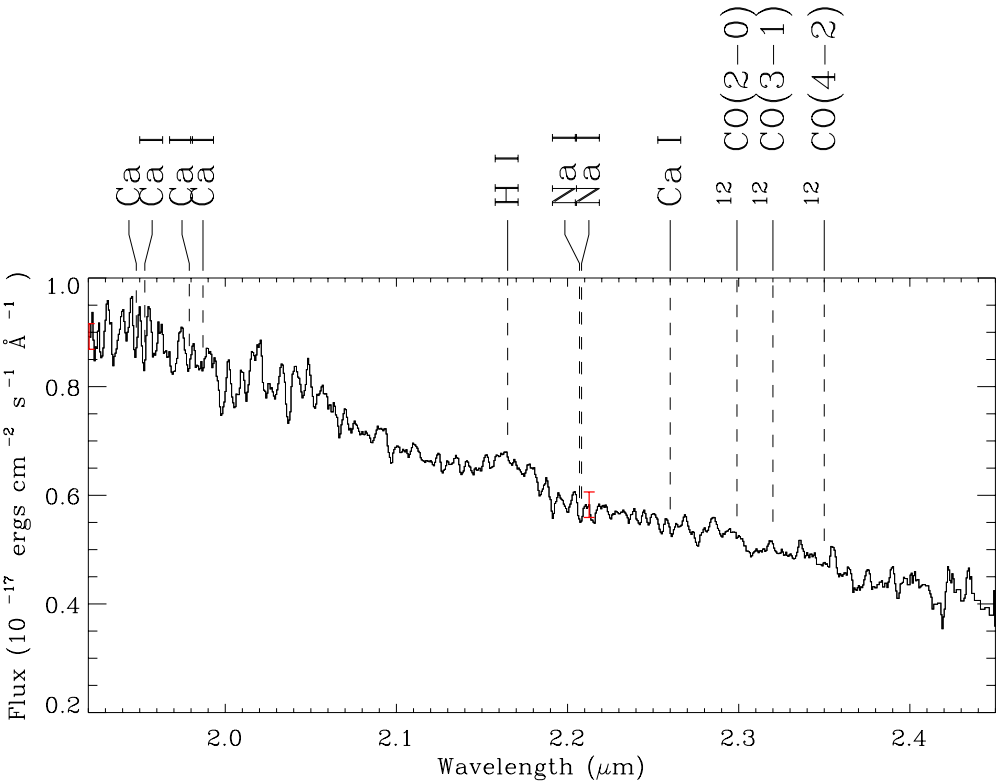

Figure 4. *K*-band spectrum of XTE J1118+480.
(A color version of this figure is available in the online journal.)

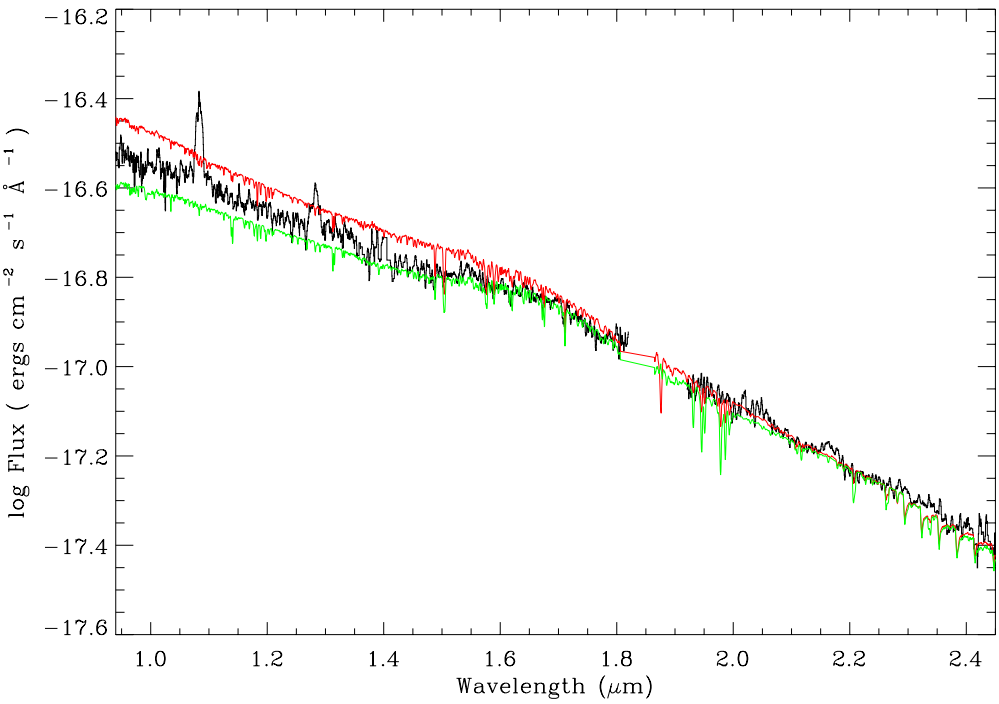

Figure 5. Time-averaged spectrum of XTE J1118+480 compared to the spectrum of a K5 V star (in red) and an M1 V star (in green). The K5 V and M1 V spectra have been scaled to match the XTE J1118+480 flux near 2.23 μm.
(A color version of this figure is available in the online journal.)

sources will have the effect of decreasing the equivalent widths of the lines in the observed spectrum compared to those in the templates. By scaling the templates to fit the observed line strengths, we can determine the donor star fractional contribution to the NIR spectrum of XTE J1118+480.

To normalize the spectra, we fit a spline function to the continuum, which was then divided out. The continuum points were selected by eye. The normalized spectrum of the template star was scaled by a fraction f that was varied from 0 to 1 in steps of 0.01. The normalized, scaled template was subtracted

Table 2
Donor Star Fraction Fits

Band	Wavelength Range (μm)	Dominant Feature	f(K5 V)	f(K7 V)	f(M0.5 V)	f(M1 V)
K	2.203–2.214	Na I	0.80 ± .15	0.70 ± .15	0.65 ± .18	0.62 ± .18
H	1.48–1.51	Mg I	0.37 ± .07	0.37 ± .07	0.48 ± .08	0.58 ± .09
	1.568–1.60	Mg I, Si I	0.40 ± .11	0.44 ± .09	0.47 ± .09	0.63 ± .10
	1.67–1.68	Al I	0.39 ± .12	0.39 ± .11	0.30 ± .09	0.40 ± .10
	1.70–1.72	Mg I	0.55 ± .09	0.60 ± .09	0.65 ± .11	0.70 ± .09
J	1.176–1.202	Mg I, Fe I, Si I	0.63 ± .10	0.65 ± .13	0.68 ± .13	0.69 ± .15
	1.310–1.317	Al I	0.65 ± .15	0.64 ± .16	0.66 ± .17	0.72 ± .18

from the normalized spectrum of XTE J1118+480 and the residual was computed. The value of f that minimized the deviation between the residual and the mean of the residual determined the best fit. For the template spectra, we used stars of spectral type K5 V (HD36003), K7 V (HD237903), M0/M0.5 V (HD209290), and M1 V (HD42581; there is a disagreement in literature about the spectral type of HD209290 and hence we refer to it as M0/M0.5 V star, Rayner et al. 2009; Koen et al. 2010). The template star spectra were obtained from the IRTF spectral library.[7]

The fit regions that were investigated in the *J, H,* and *K* bands for the spectral types between K5 V and M1 V are listed in Table 2 along with the best-fit donor fractions, f, and uncertainties on those values. In the *J* band, our fits were restricted to the region between 1.20 and 1.314 μm within which we detected features containing blends of Mg I, Si I, Fe I, and Al I. In the *H* band, we fit features of Mg I, Al I, and Si I over the wavelength range 1.475–1.73 μm. We only show fits in the *K* band to the Na I feature, although the detection of this line is marginal.

Since the S/N in our spectrum is low and the use of χ^2 statistics for the spectral fitting is affected by systematic uncertainties (see the discussion in Froning et al. 2007), we have adopted a new technique to properly evaluate the noise associated with the spectrum of XTE J1118+480 and its contribution to the donor fractions. The procedure for this involves "scrambling" the XTE J1118+480 spectrum and fitting the template star spectra to many such randomly "scrambled" spectra in order to place robust error estimates on the best-fit donor fractions. A detailed explanation can be found in the Appendix. The uncertainties calculated in this manner are shown in Table 2.

We also examined if the calculated donor fractions were consistent with the overall shape of the broadband SED of XTE J1118+480. To answer that question, we scaled the flux of each field star by the average donor fraction in the *H* band (near 1.6 μm) and computed the value by which the average flux of the scaled template spectrum drops below that of XTE J1118+480 in both the *J* and *K* bands. Less emphasis was given to obtaining a *K*-band match due to the fact that we only had the Na I feature to compare with, and this feature is at about the same level as the noise in the *K* band. Depending on whether the corresponding drop in flux in the *J* band was consistent with the average *J*-band donor fraction (within the bounds allowed by propagating the errors to calculate the average donor fraction) computed from Table 2, we could further constrain the donor spectral type. When a K5 V star was scaled to 43% of the XTE J1118+480 flux at the center of the *H* band, it resulted in an average flux drop of 41% in the *J* band (between 1.1 and 1.3 μm) and 38% in the *K* band (near 2.20 μm), inconsistent with the average donor fractions expected from the fits to lines in those bands. A K7 V matches the drop in *J*-band flux but not in the *K* band, while M0.5 V/M1 V matches both the *J* and *K* bands when their *H*-band fluxes were scaled to the corresponding average *H*-band donor fraction obtained from Table 2. This suggests that K7–M1 V is the most likely range of donor spectral types in XTE J1118+480. This is also consistent with the shape of the broad *H*-band bump near 1.6 μm discussed above.

Thus, we conclude that the spectral type best describing the donor star in XTE J1118+480 lies between K7 V and M1 V. We estimate the donor fraction by averaging the best fits to multiple lines using the K7–M1 V templates and propagating the corresponding uncertainties from Table 2. This leads to a *H*-band donor contribution of $f = 0.50 \pm 0.32$ in the spectrum of XTE J1118+480 at the epoch of our observations. The upper panel of Figure 6 shows the normalized spectrum of XTE J1118+480 plotted (in black) over the normalized spectrum of a K7 V star (in red) while the lower panel shows the same comparison but with the K7 V star scaled to match the best donor fraction of 50%.

3.2. Modeling the Light Curve to Obtain the Inclination

Our spectroscopic observations of XTE J1118+480 were obtained in conjunction with contemporaneous light curve data. We phase-binned the *H*-band observations using the orbital ephemeris from Gonzalez Hernandez et al. (2008). Figure 7 shows the *H*-band light curve after the data were combined into orbital phase bins of size $\Delta\phi = 0.03$. Each datum in the figure represents the mean of the points in the specific phase bin. The error bars are the rms scatter of the points about the mean in each bin. In cases where we did not have enough data points (<3) to place a reliable error estimate on the magnitude, the error bar for that datum was changed to the value of the largest error bar for the other light curve points. The orbital phases represent the standard convention wherein phase 0.0 is inferior conjunction of the donor star.

The *H*-band light curve in Figure 7 shows a departure from the conventional ellipsoidal modulation expected from a Roche lobe-filling donor star: the maximum at phase $\phi = 0.75$ is higher than the maximum at $\phi = 0.25$. Similar asymmetric modulations were detected in the quiescent *J*-band light curve of XTE J1118+480 obtained by Mikolajewska et al. (2005). However, Gelino et al. (2006) obtained NIR light curves of XTE J1118+480 four months prior to Mikolajewska et al. (2005) and found no asymmetries in their NIR light curves. Typically, this observed asymmetry in the light curve maxima is attributed to the emission from a bright spot in the accretion disk (Froning & Robinson 2001) or from a dark spot on the donor

[7] http://irtfweb.ifa.hawaii.edu/~spex/IRTF_Spectral_Library

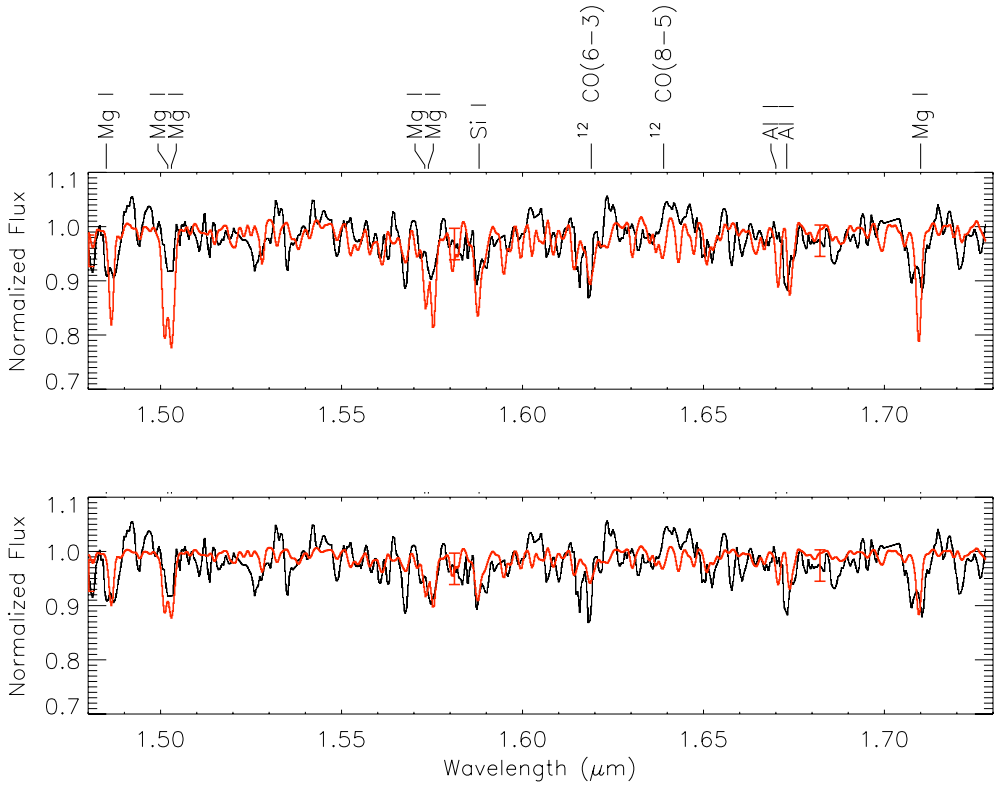

Figure 6. Normalized *H*-band spectrum of XTE J1118+480 is shown in the upper panel with the normalized spectrum of a K7 V star overplotted (in red). The lower panel shows the same spectra after the K7 V star has been normalized to the best-fit fractional contribution of 0.50.
(A color version of this figure is available in the online journal.)

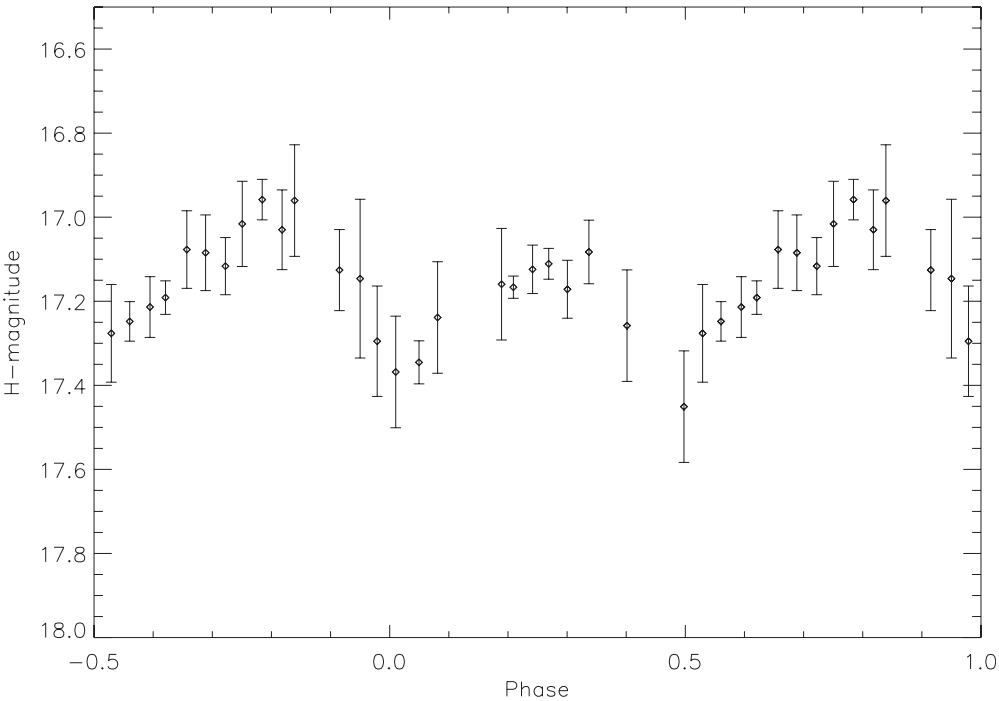

Figure 7. Light curve of XTE J1118+480 after binning the observed data in phase bins of 0.03. The error bars are derived from scatter about the mean in each bin. For phase bins that contained fewer than three points, we used the largest error bar in the rest of the bins as the uncertainty.

star (Gelino et al. 2001). Evidence for the presence of a hot spot in XTE J1118+480 is ambiguous: Doppler and modulation tomography of XTE J1118+480 taken during quiescence by Calvelo et al. (2009) revealed a well-defined hot spot, but Torres et al. (2004) found no evidence of a hot spot in their Doppler tomograms. Calvelo et al. (2009) speculated that variations in the mass transfer rate from the donor star during quiescence may cause the bright spot to be intermittent.

In the following sections, we present two simple models for fitting the observed light curve of XTE J1118+480:

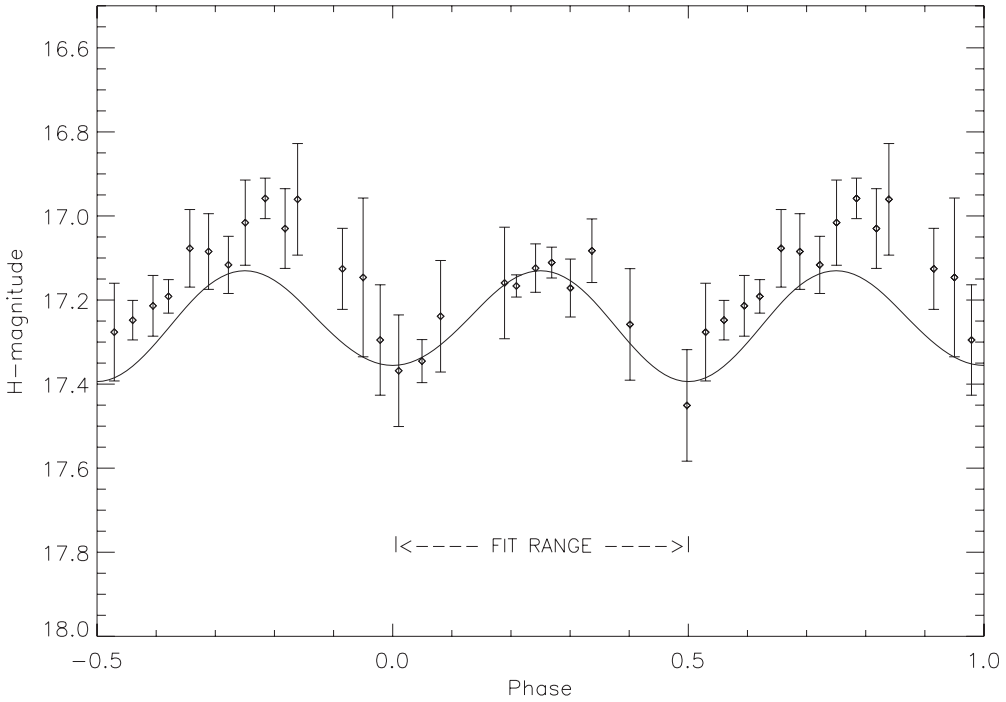

Figure 8. Best-fit light curve obtained by modeling a donor star (fit range: $\phi = 0.0$–0.5) with a constant extra flux component. The inclination is 68°.

(1) a model incorporating a donor star with constant extra flux from nonstellar sources (e.g., the accretion disk and/or a jet) and (2) a model incorporating a donor star and an accretion disk with a bright spot. We modeled the *H*-band light curve of XTE J1118+480 using an updated version of the light curve synthesis code first presented in Zhang et al. (1986) that has been used to model the light curves in several other LMXBs (Froning & Robinson 2001; Khargharia et al. 2010). The code accounts for the geometry of the binary system and then calculates the light curve by computing the temperature and intensity distribution across the surface of the Roche lobe-filling donor star and an accretion disk with a bright spot. It also takes into account gravity and limb darkening for each component of the system. The best-fit light curve is obtained by minimizing the chi-squared value between the synthetic and the observed light curves. Below, we discuss each model that was fitted to the observed light curve of XTE J1118+480.

3.2.1. Modeling the H-band Light Curve with a Donor Star and Constant Non-stellar Flux

We ran models to evaluate the effect of adding constant (i.e., present over the full binary orbit) non-stellar flux on the inclination of the binary. For modeling purposes, the donor star parameters were set as follows: $T_{\rm eff} = 4000$ K, to reflect the average temperature from the spectral type range determined above; a gravity darkening coefficient of 0.08, assuming that the donor has a convective envelope (Lucy 1967; Sarna 1989); and limb-darkening coefficients from Claret et al. (1995). We adopted the mass ratio value obtained by Calvelo et al. (2009), which agrees with past estimates obtained by Gonzalez Hernandez et al. (2008), Torres et al. (2004), and Zurita et al. (2002). To avoid the extra flux at $\phi = 0.75$, we modeled the light curve between phases $\phi = 0.0$–0.50 only. By allowing the constant non-stellar fraction $(1 - f)$ to vary within the limits obtained from spectroscopy, we modeled the light curve data to derive the corresponding best-fit binary inclinations. Using this method, we find the binary inclination to lie between 68° and 89°. Figure 8 shows the best-fit light curve ($i = 68°$) obtained by modeling the observed light curve with a donor star and for a disk light fraction of $f_{\rm disk} = 0.18$ ($\chi^2_\nu = 0.51$). We varied the mass ratio within the limits specified in Calvelo et al. (2009) and the results were unchanged. From this, we conclude that accounting for the non-stellar flux within its uncertainty bounds obtained from spectroscopy places a lower limit on the binary inclination of $i \geqslant 68°$.

3.2.2. Modeling the H-band Light Curve with a Donor Star and an Accretion Disk with a Bright Spot

The *H*-band light curve of XTE J1118+480 shows asymmetry in the maxima of the peaks at phases 0.25 and 0.75, which is often attributed to emission from a bright spot on the accretion disk. Accordingly, we also fit the light curve with a model that includes a donor star and a cool opaque accretion disk with a bright spot on its rim. By this method, we do not attempt to constrain the physical properties associated with either the disk or the bright spot. (Indeed, there is no a priori reason to believe that the non-variable emission comes from the accretion disk rather than partially or wholly from a persistent jet.) However, we can derive a range of possible inclinations by modeling this system with reasonable estimates for the parameters associated with the accretion disk and bright spot.

The donor star parameters were set at the same values used in the earlier models. Varying the donor star parameters had a negligible effect ($\leqslant 1°$ change) on the derived inclination of the system, and therefore we keep them fixed for this set of models and only vary the parameters associated with the accretion disk and the bright spot. For the accretion disk, we adopted an inner radius of 0.001 R_{L_1} (where R_{L_1} represents the distance to the inner Lagrangian point) and an outer disk radius of 0.75 R_{L_1}; these numbers are taken from the work done by Wren et al. (2001) and Calvelo et al. (2009). We set the flare half-angle of the disk to a small value of 1°. The bright spot was added to the

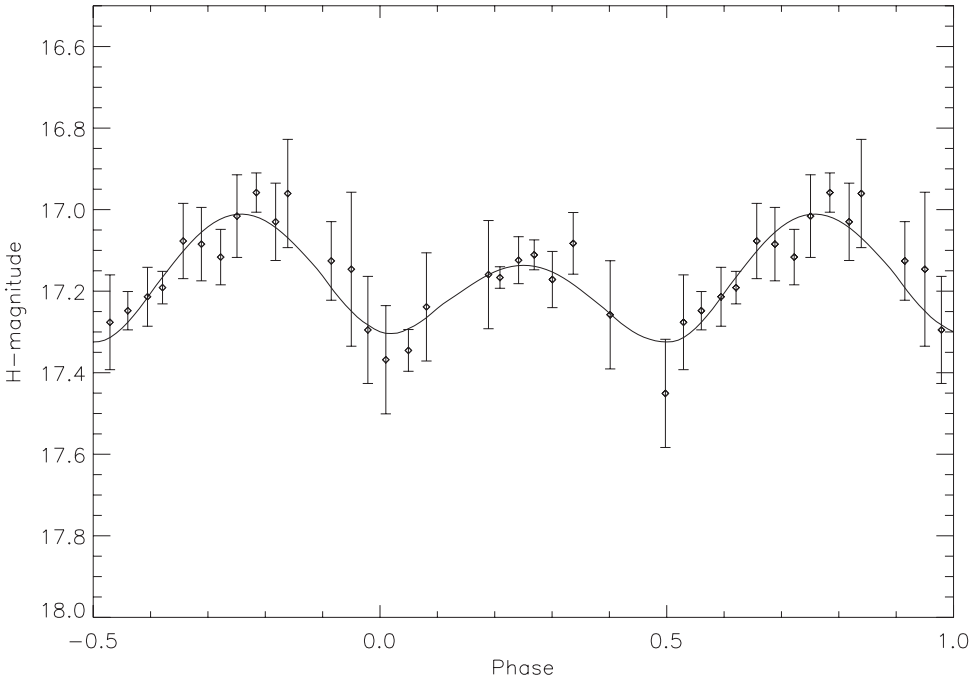

Figure 9. Light curve models consisting of a donor star and an accretion disk along with a bright spot are fit to the full light curve of XTE J1118+480. The best-fit parameters for this model are $i = 78^\circ$, $T_{\rm disk} = 3000$ K, $T_{\rm spot} = 12000$ K, $\phi_{\rm spot} = 85^\circ$, and $\Delta\phi_{\rm spot} = 5^\circ$.

rim of the disk and spans an angle in the azimuthal direction whose position $\phi_{\rm spot}$ and width $\Delta\phi_{\rm spot}$ are variable parameters in the light curve fitting model. The other input parameters are the temperature of the disk ($T_{\rm disk}$) and the bright spot ($T_{\rm spot}$). Both the accretion disk and the bright spot were assumed to emit as black bodies with single temperatures and linear limb-darkening coefficients. We varied $T_{\rm disk}$ between 2500 and 4500 K, $T_{\rm spot}$ from 5000 to 20000 K, $\phi_{\rm spot}$ from 40° to 120°, and $\Delta\phi_{\rm spot}$ from 5° to 15°. The choice of $T_{\rm disk}$ was motivated by the work done in Reynolds et al. (2008), who found that thermal emission from a cool outer accretion disk ($T_{\rm disk} \sim$ 2000–4000 K) could be used to model the excess NIR emission in the multi-wavelength SED of several X-ray backgrounds (including XTE J1118+480).

Using these parameters, we fit models to the full *H*-band light curve. In Figure 9, we show the best-fit light curve ($\chi^2_\nu = 0.57$), with an inclination of 78°, $T_{\rm disk} = 3000$ K, $T_{\rm spot} = 12000$ K, $\phi_{\rm spot} = 85^\circ$, and $\Delta\phi_{\rm spot} = 5^\circ$. From an investigation of our fits over the entire range of input parameters, we find that all of the fits have χ^2_ν values between 0.60 and 0.80 and produced lower/higher $T_{\rm disk}$ values for correspondingly lower/higher $T_{\rm spot}$ values; e.g., a model with $T_{\rm disk} = 2500$ K and $T_{\rm spot} = 10000$ K for an inclination of $i = 74^\circ$ gave a comparable fit ($\chi^2_\nu = 0.60$) to a model with $T_{\rm disk} = 4000$ K and $T_{\rm spot} = 13000$ K for an inclination for $i = 81^\circ$ ($\chi^2_\nu = 0.63$).

We do not attempt to set constraints on either the disk or the bright spot parameters based on the light curve models with the lowest χ^2_ν value, except to note that a simple model incorporating a donor star and an accretion disk with a bright spot on the rim can account for the extra flux at $\phi = 0.75$. More importantly, we can set an upper limit on the binary inclination through the absence of eclipse features in the light curve. Extensive multiwavelength observations of XTE J1118+480 in outburst found no evidence of eclipses in this system (Uemura et al. 2000; Wood et al. 2000). From our modeling, we find that eclipse features start to emerge in the model light curves at $i \geqslant 80^\circ$ for an accretion disk of outer radius 0.75 R_L. Hence, to maintain consistency with the non-detection of eclipses in XTE J1118+480, we find an upper limit to the binary inclination of $\leqslant 79^\circ$.

Table 3
Adopted Physical Parameters for XTE J1118+480

Parameter	Value	Reference
$P_{\rm orb}$	0.16995 ± 0.00012 d	González Hernández et al. (2008)
K_2	708.8 ± 1.4 km s^{-1}	Ibid
q	0.024 ± 0.009	Calvelo et al. (2009)
i	68°–79°	This work
$M_{\rm BH}$	6.9–8.2 $M_\odot$	This work
Donor spectral type	K7 V–M1 V	This work

In modeling asymmetric light curve peaks in X-ray binaries, some authors have attributed the asymmetry to a dark spot on the donor star rather than a bright spot on the accretion disk (Gelino et al. 2001). In that case, our assumption in the previous section that modeling orbital phases $\phi = 0.0$–0.50 is preferable to modeling the full light curve is exactly backward and we would have underestimated the true amplitude of the ellipsoidal modulation (as we would then be modeling the hump artificially depressed by the stellar spot). If so, then our lower limit to the inclination of $\geqslant 68^\circ$ is conservative but still encompasses the higher inclination that would result from fitting the larger hump in the light curve.

In summary, by modeling the observed light curve with a constant non-stellar fraction obtained from spectroscopy, we found a lower limit to the binary inclination in XTE J1118+480 as $\geqslant 68^\circ$. Additionally, an upper limit on the inclination is dictated by the absence of eclipses, as $<80^\circ$. Hence, we have constrained the binary inclination to lie between $68^\circ \leqslant i \leqslant 79^\circ$.

4. DISCUSSION

In Table 3, we summarize the current best estimates for the physical parameters including the black hole mass for XTE J1118+480. By performing spectroscopy of

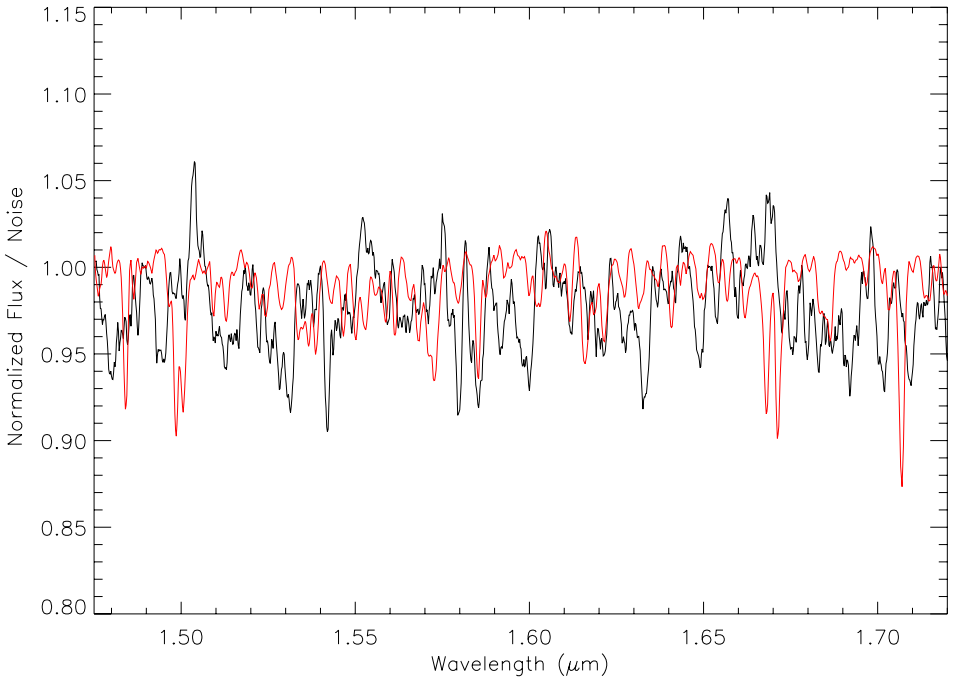

Figure 10. Example of fitting an M0.5 V stellar spectrum to the inverse "phase scrambled" Fourier-transformed spectrum of XTE J1118+480. The donor fraction variance obtained from fitting many such randomly phase-scrambled spectra was used to place uncertainties on the donor star fraction.

(A color version of this figure is available in the online journal.)

XTE J1118+480, we find that the donor star contributes a fraction $f = 0.50 \pm 0.32$ of the H-band flux. By varying the constant non-stellar fraction within the limits obtained from the spectroscopy while simultaneously imposing the absence of eclipse condition, we obtained a binary inclination of $68^\circ \leqslant i \leqslant 79^\circ$. Using this inclination range, combined with the orbital parameters from Calvelo et al. (2009), we find the mass of the black hole in XTE J1118+480 to be $6.9 \leqslant (M_{\rm BH}/M_\odot) \leqslant 8.2$. Previous analyses have found inclinations ranging from $i = 60^\circ$ to $i = 82^\circ$ (Frontera et al. 2001; Zurita et al. 2002; Mikolajewska et al. 2005; Khruzina et al. 2005; Gelino et al. 2006). Unfortunately, because of the relatively low S/N of our spectrum, we were only able to constrain the donor star fraction broadly. Despite that, the binary inclination range we found was fairly narrow (12°) and we were able to provide a new constraint on the mass of the black hole in XTE J1118+480. Interestingly, the binary inclination of $68^\circ \pm 2^\circ$ determined by Gelino et al. (2006) is at the low edge of our inclination range, suggesting that they may have acquired their light curve data when the NIR non-stellar contribution was small.

In an extensive study of the X-ray binary A0620-00, Cantrell et al. (2008, 2010) showed that the system existed in three distinct optical states even in quiescence. The authors found that a correct determination of the inclination relies on identifying the state of the system. This was found to be more important than the particular waveband where the measurements are made since non-stellar sources were present at both optical and NIR wavelengths. XTE J1118+480 also exhibits changes in the shape of its quiescent ellipsoidal light curve (e.g., comparing the data of Gelino et al. 2006 and Mikolajewska et al. 2005). The asymmetry we observed in the H-band light curve of XTE J1118+480 is similar to that seen by Mikolajewska et al. (2005) in their J-band data. Significant changes in the quiescent infrared light curves of the black hole X-ray binary GRO J0422+32 were also seen in two independent observations by Reynolds et al. (2007) and Gelino & Harrison (2003) even though the mean K-band magnitudes did not vary significantly. From these studies, it is clear that X-ray binary systems continue to harbor extensive activity and multiple accretion and/or outflow states even when fully in quiescence.

5. CONCLUSIONS

We have obtained broadband near-infrared spectroscopy of XTE J1118+480 and contemporaneous light curve data to accurately account for the veiling that affects determinations of the binary inclination and compact object mass. By comparing the shape of the SED of the combined NIR spectrum as well as individual absorption lines in our spectrum with those of field stars of known spectral type, we were able to broadly account for the fraction of NIR light contributed by the donor star as $f = 0.50 \pm 0.32$. We factored the non-stellar contribution into our H-band light curve fits and obtained a binary inclination of $68^\circ \leqslant i \leqslant 79^\circ$. From these, we obtained a robust determination of the black hole mass in XTE J1118+480 of $6.9 < (M_{\rm BH}/M_\odot) \leqslant 8.2$. Our results are consistent with the picture of continued activity in X-ray binary systems even in quiescence and underscore the importance of accounting for all emission sources in the binary system when modeling spectra and light curves, even at NIR wavelengths.

We thank Emma Hogan for her assistance with Gemini-IRAF and Bernadette Rogers for letting us use her code to make GNIRS data compatible for use with Spextool.

Facilities: Gemini:Gillett (GNIRS), ARC (NICFPS)

APPENDIX

DETERMINATION OF ERROR IN THE DONOR FRACTION CALCULATION

Due to the low S/N of our spectrum, the donor fraction obtained from the spectrum of XTE J1118+480 is only meaningful

if accompanied by reliable uncertainty estimates. In order to adequately account for the noise in the spectrum, we created "scrambled" versions of the observed spectrum and used fits to the noise spectra to determine the uncertainties on the donor star fraction. For each of the *J*-, *H*-, and *K*-band spectra, we obtained the Fourier transform of the normalized spectrum. The Fourier-transformed spectra give a complex valued array, $X(k) = \sum_{n=1}^{N} x(n) e^{(-2\pi i/N)(n-1)k}$, where N represents the total data points, k represents the individual Fourier transformed frequency components, and $x(n)$ represents the normalized flux values. The amplitude of the Fourier transform is given by $A(k) = (\mathrm{Re}[X(k)]^2 + \mathrm{Im}[X(k)]^2)^{1/2}$ and the phase is given by $\phi(k) = \tan^{-1}(-(\mathrm{Im}(X(k)))/(\mathrm{Re}(X(k))))$.

To estimate the noise in our spectral data, we "scrambled" the phase of the Fourier-transformed spectrum by adding a different random number between 0 and 2π to the original phase at each k while retaining the original power spectrum $|X_k|^2$. We used the `rand` function in MATLAB that generates uniformly distributed random numbers between zero and one. We then reconstructed the spectrum by calculating the inverse Fourier transform of the "phase scrambled" Fourier-transformed spectrum. In Figure 10, we depict an example of calculating the donor fraction when an M0.5 V star was compared to the reconstructed "phase scrambled" spectrum of XTE J1118+480 in the *H* band.

The advantage of scrambling the phases in Fourier space is that, unlike scrambling the original wavelength-binned data, it works for both white and non-white noise. Any fit done to the "phase scrambled" spectrum will be spurious since we are fitting signal to pure noise which allows us to place uncertainties on our fits to the original spectrum. We fitted the spectra of field stars with K5 V, K7 V, M0/M0.5 V, and M1 V spectral types to each of the phase scrambled spectra and calculated the donor fraction for each wavelength region under investigation listed in Table 2. For each field star and each wavelength region under investigation, we repeated this process for 50 randomly generated phase scrambled spectra and examined the variance of the donor fractions. The square root of the variance is then a robust indication of the uncertainty in the donor star fraction. The errors listed with the donor fractions in Table 2 were obtained from this analysis. Finally, these errors were propagated through the remainder of the steps leading up to the average donor fractions in the *J*, *H*, and *K* bands.

REFERENCES

Belczynski, K., Wiktorowicz, G., Fryer, C. L., Holz, D. E., & Kalogera, V. 2012, ApJ, 757, 91
Brown, E. F., Bildsten, L., & Rutledge, R. E. 1998, ApJ, 504, L95
Calvelo, D. E., Vrtilek, S. D., Steeghs, D., et al. 2009, MNRAS, 399, 539
Cantrell, A. G., Bailyn, C. D., McClintock, J. E., & Orosz, J. A. 2008, ApJ, 673, L159
Cantrell, A. G., Bailyn, C. D., Orosz, J. A., et al. 2010, ApJ, 710, 1127
Chaty, S., Haswell, C. A., Malzac, J., et al. 2003, MNRAS, 346, 689
Claret, A., Diaz-Cordoves, J., & Gimenez, A. 1995, A&AS, 114, 247
Cushing, M. C., Vacca, W. D., & Rayner, J. T. 2004, PASP, 116, 362
Elias, J. H., Rodgers, B., Joyce, R. R., et al. 2006, Proc. SPIE, 6269, 138
Falcke, H., Körding, E., & Markoff, S. 2004, A&A, 414, 895
Fender, R. P., Hjellming, R. M., Tilanus, R. P. J., et al. 2001, MNRAS, 322, L23
Fragos, T., Willems, B., Kalogera, V., et al. 2009, ApJ, 697, 1057
Froning, C. S., & Robinson, E. L. 2001, AJ, 121, 2212
Froning, C. S, Robinson, E. L., & Bitner, M. A. 2007, ApJ, 663, 1215
Frontera, F., Zdziarski, A. A., Amati, L., et al. 2001, ApJ, 561, 1006
Fryer, C. L., & Kalogera, V. 2001, ApJ, 554, 548
Gelino, D. M., Balman, Ş., Kiziloğlu, Ü., et al. 2006, ApJ, 642, 438
Gelino, D. M., & Harrison, T. E. 2003, ApJ, 599, 1254
Gelino, D. M., Harrison, T. E., & Orosz, J. A. 2001, AJ, 122, 2668
Gonzalez Hernandez, J. I., Rebolo, R., Israelian, G., et al. 2008, ApJ, 679, 732
Haswell, C. A., Hynes, R. I., King, A. R., & Schenker, K. 2002, MNRAS, 332, 928
Hearty, F., Beland, S., Green, J., et al. 2005, Proc. SPIE, 5904, 199
Hunt, L. K., Mannucci, F., Testi, L., et al. 1998, AJ, 115, 2594
Hynes, R. I., Mauche, C. W., Haswell, C. A., et al. 2000, ApJ, 539, L37
Johannsen, T. 2009, A&A, 507, 617
Khargharia, J., Froning, C. S., & Robinson, E. L. 2010, ApJ, 716, 1105
Khruzina, T. S., Cherepashchuk, A. M., Bisikalo, D. V., Boyarchuk, A. A., & Kuznetsov, O. A. 2005, ARep, 49, 79
Koen, C., Kilkenny, D., van Wyk, F., & Marang, F. 2010, MNRAS, 403, 1949
Kreidberg, L., Bailyn, C. D., Farr, W. M., & Kalogera, V. 2012, ApJ, 757, 36
Lucy, L. B. 1967, ZA, 65, 89
Maitra, D., Markoff, S., Brocksopp, C., et al. 2009, MNRAS, 398, 1638
McClintock, J. E., Garcia, M. R., Caldwell, N., et al. 2001a, ApJ, 551, L147
McClintock, J. E., Haswell, C. A., Garcia, M. R., et al. 2001b, ApJ, 555, 477
McClintock, J. E., Narayan, R., Davis, S. W., et al. 2011, CQGra, 28, 114009
Merloni, A., Heinz, S., & di Matteo, T. 2003, MNRAS, 345, 1057
Mikolajewska, J., Rutkowski, A., Gonclaves, D. R., & Szostek, A. 2005, MNRAS, 362, L13
Nelemans, G., & van dan Heuval, E. P. J. 2001, A&A, 376, 950
Rayner, J. T., Cushing, M. C., & Vacca, W. D. 2009, ApJS, 185, 289
Remillard, R., Morgan, E., Smith, D., & Smith, E. 2000, IAU Circ., 7389, 2
Reynolds, M. T., Callanan, P. J., & Filippenko, A. V. 2007, MNRAS, 374, 657
Reynolds, M. T., Callanan, P. J., Robinson, E. L., & Froning, C. S. 2008, MNRAS, 387, 788
Sarna, M. J. 1989, A&A, 224, 98
Steiner, J. F., McClintock, J. E., Remillard, R. A., Narayan, R., & Gou, L. 2009, ApJ, 701, L83
Torres, M. A. P., Callanan, P. J., Garcia, M. R., et al. 2004, ApJ, 612, 1026
Uemura, M., Kato, T., Matsumoto, K., et al. 2000, PASJ, 52, L15
Vacca, W. D., Cushing, M. C., & Rayner, J. T. 2003, PASP, 115, 389
Wagner, I. M., Foltz, C. B., Shahbaz, T., et al. 2001, ApJ, 556, 42
Wood, K. S., Ray, P. S., Bandyopadhyay, R. M., et al. 2000, ApJ, 544, L45
Wren, J., Akerlof, C., Balsano, R., et al. 2001, ApJ, 557, L97
Yuan, F., Cui, W., & Narayan, R. 2005, ApJ, 620, 905
Zhang, E. H., Robinson, E. L., & Nather, E. R. 1986, ApJ, 305, 740
Zurita, C., Casares, J., Shahbaz, T., et al. 2002, MNRAS, 333, 791